Computers and Concrete, *Vol. 25, No. 5* (*2020*) *461-470*
DOI: https://doi.org/10.12989/cac.2020.25.5.461

Numerical analysis of RC hammer head pier cap beams extended and reinforced with CFRP plates

Cheng Tan[a], Jia Xu[b] and Riyad S. Aboutaha*

Department of Civil and Environmental Engineering, Syracuse University, 151 Link Hall, Syracuse, NY 13244, USA

(*Received May 17, 2019, Revised April 21, 2020, Accepted April 30, 2020*)

Abstract. This paper presents a numerical study on structural behavior of hammer head pier cap beams, extended on verges and reinforced with carbon fiber reinforced polymer (CFRP) plates. A 3-D finite element (FE) model along with a simplified analytical model are presented. Concrete damage plasticity (CDP) was adapted in the FE model and an analytical approach predicting the CFRP anchor strength was adapted in both FE and analytical model. Total five quarter-scaled pier cap beams with various CFRP reinforcing schemes were experimentally tested and analyzed with numerical approaches. Comparison between experimental results, FE results, analytical results and current ACI guideline predictions was presented. The FE results showed good agreement with experimental results in terms of failure mode, ultimate capacity, load-displacement response and strain distribution. In addition, the proposed strut-and-tie based analytical model provides the most accurate prediction of ultimate strength of extended cap beams among the three numerical approaches.

Keywords: pier cap beam; extensions; finite element method; CFRP; strut-and-tie model

1. Introduction

Hammer head concrete piers are widely used as support for highway bridges. In order to increase lane width, or handle larger volume of traffic, some of these bridges are in need of widening. Current practice for widening a bridge is accomplished by addition of side piers, along with un-connected new superstructure. However, for bridges in congested cities, the addition of new columns is not practical, as it blocks side access roads. In that case, extending the pier cap beam is the only practical solution, despite the potential high cost of foundation strengthening. Recently, two bridges have been widened without the addition of new columns: Tongati River Bridge and Olifants River Bridge, in South Africa (KwaZulu-Natal Department of Transport 2017, Rowan and Thomson 2018). Pier cap beams of the bridges were extended on both sides and strengthened with post-tensioned dowel bars.

Several strengthening systems could be adopted for extended pier cap beams, e.g., external prestressing and ordinary reinforced concrete jacketing. External prestressing has been used world-wide for repair of cracked pier cap beams, as it is a very effective system for closing opened cracks. However, in corrosive environments, the steel prestressing bars are subjected to the environment, and require corrosion protection system to ensure long service life. Carbon fiber reinforced polymer (CFRP) composites have been widely used for bridge strengthening. Applications included flexural and shear strengthening of girders, axial and shear strengthening of circular pier columns, and seismic strengthening of pier columns for improved ductility. Hag-Elsafi *et al*. (2002) strengthened a reinforced concrete bridge pier cap beam in both shear and flexure (positive and negative moment) and tested the beam under service load. Test results indicated that FRP composites moderately reduced the live load stresses on steel reinforcement. It has been proven that FPR composites are effective in strengthening concrete pier cap beams under both positive and negative moments. Further analysis (Eamon *et al*. 2012) shows that FRP strengthening systems are cost-effective and cause minimal interruption to traffic.

Numerical simulation of CFRP strengthened reinforced concrete (RC) members with finite element method has been extensively studied (Biolzi *et al*. 2013, Zhang 2016, Mostafa and Razaqpur 2017, Jawdhari and Harik 2018). Two challenging issues in FE modelling of CFRP strengthened RC members are concrete cracking behavior and bond-slip relation at CFRP-concrete interface. The discrete and the smeared approaches are the two dominant techniques for fracture simulation of concrete. Both approaches are capable of simulating failure modes such as intermediate crack induced debonding and concrete cover separation failure. On the other hand, many approaches were developed to simulate the bond behavior at FRP-concrete interface, the most commonly used three approaches are: 1) fully bond; 2) nonlinear spring between concrete adhesive layers (Luo *et al*. 2012); 3) interface element (Wu *et al*. 2009). The fully bond approach is sensitive to accuracy of concrete property and mesh. The non-linear spring and interface element approach require

*Corresponding author, Associate Professor
E-mail: rsabouta@syr.edu
[a]Ph.D.
E-mail: ctan@syr.edu
[b]Ph.D. Student
E-mail: jxu26@syr.edu

http://www.techno-press.org/?journal=cac&subpage=8
ISSN: 1598-8198 (Print), 1598-818X (Online)

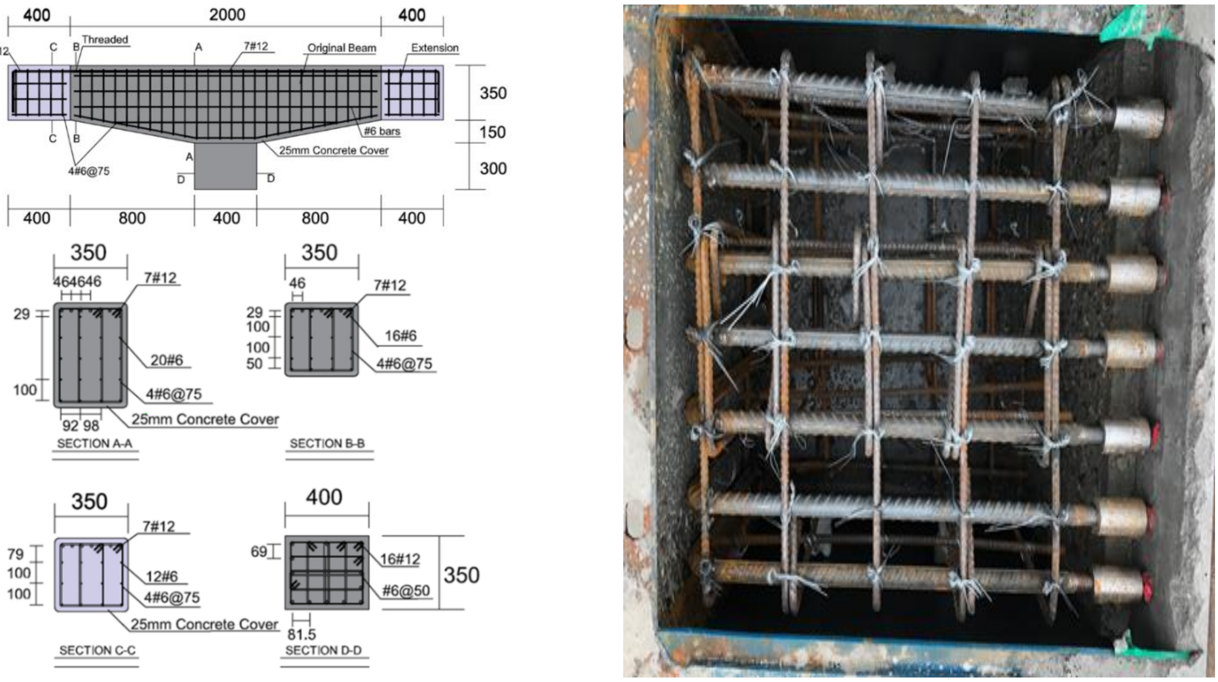

(a) (b)

Fig. 1 Detailing of reference specimen (Dimensions in mm)

input of an appropriate bond-slip model of FRP-concrete interface.

Other than finite element method, numerous analytical approaches were developed to predict capacity of FRP strengthened RC beams. AASHTO (2012) and ACI (2017) provide similar sectional approaches to determine flexural capacity of FRP strengthened beams. However, pier cap beams are generally deep beams, even though in this study, span-to-depth-ratio of the cap beams were increased by the extensions. Among numerous analytical approaches for deep analysis (Lu *et al*. 2010, Rafeeqi and Ayub 2012, Mihaylov *et al*. 2013), strut-and-tie model is one of the most commonly used method to predict ultimate capacity of RC deep beams. Application of strut-and-tie model on CFRP reinforced deep beams was investigated (Andermatt and Lubell 2013, Thomas and Ramadass 2019, Park and Aboutaha 2009, Panjehpour 2014), however, these models rarely predict the post-failure such as anchor failure.

This paper presents a finite element model which is capable of simulating structural behavior of extended pier cap beams reinforced with prefabricated CFRP plates. Experimental results of five specimens with various reinforcing schemes were used to verify the proposed FE model. In addition, an iterative strut-and-tie model was developed to predict ultimate capacity of the extended pier cap beams.

2. Experimental tests

This experimental program aimed to investigate the effectiveness of various CFRP strengthening systems used on extended cap beams. A total of five non-prismatic hammer-headed pier cap beams were constructed and tested. Fig. 1 shows the reference specimen and Fig. 2 shows the strengthening systems. The tensile reinforcement in existing beam and the extensions was threaded and connected using straight threaded sleeves, as shown in Fig. 1(b). The surfaces were roughened before cast of the extensions.

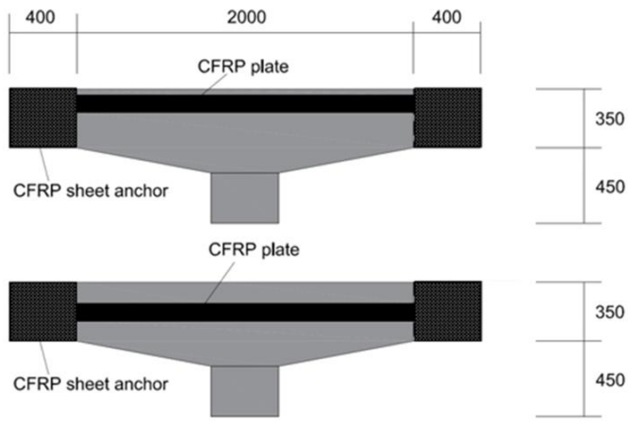

Fig. 2 CFRP strengthening systems (Dimensions in mm)

Details of the test specimens are shown in Table 1. BREF is the reference beam, without any strengthening system. B1L1 was strengthened using one layer of CFRP plate at location 1(L1) on each side. In addition, the CFRP plates were anchored using six layers of fully wrapped CFRP sheet in the transverse direction, and two layers of U-shaped CFRP sheets in horizontal direction. B2L1 was strengthened using two layers of CFRP plates at L1 and anchored with eight layers of CFRP sheet in both directions. B1L2 was strengthened using one layer of CFRP plates at L2 and anchored with eight layers of CFRP sheet in both directions. B2L2 was strengthened using two layers of

Table 1 Test matrix

Specimen	Layer of CFRP plates	Locations of CFRP plates	Layer of CFRP sheet anchor
BREF	N/A	N/A	N/A
B1L1	1	L1	6
B2L1	2	L1	8
B1L2	1	L2	6
B2L2	2	L2	8

Table 2 Material properties

	Tensile strength (MPa)	Elastic modulus (GPa)	Elongation at break (%)
CFRP plate	2431	162	1.61
CFRP sheet	3599	237	1.68
CFRP plate adhesive	44.64	6.64	2.60
CFRP sheet adhesive	60.96	3.03	6.22

CFRP plates at L2 and anchored with eight layers of CFRP sheet in both directions.

2.1 Materials

In this study, original specimens were made of the same batch of concrete. The concrete consisted of limestone aggregates, fly-ash, and ordinary Portland cement. The water-cement ratio was 0.36. The maximum aggregates size was 12 mm. The average concrete compressive strength was 38.1 MPa. The internal flexural and shear steel reinforcements had a nominal yield strength of 500 MPa.

The CFRP plate used for flexural strengthening was a commercial unidirectional fiber product, HM-2.0P, from Shanghai Horse Construction, having a thickness of 2 mm and a width of 100 mm. The CFRP plates were bonded to the concrete surface using CFRP plate adhesive. The CFRP sheet, HM-30 from Shanghai Horse Construction, used as end anchors, was a unidirectional carbon fiber sheet. The CFRP sheets had a dry fiber content of 300 g/m^2, and a nominal thickness of 0.167 mm. The CFRP sheets were impregnated with a low viscosity structural glue (two-part epoxy resin with a mix ratio 2:1 by weight). Mechanical properties of CFRP composites and epoxies are listed in Table 2, properties were tested according to corresponding ASTM standard.

2.2 Test procedure and instrumentation

The beams were subjected to monotonic loading at the free end of the cantilevers using two vertical positioned 1000 kN MTS actuators, as shown in Fig. 3. Load was applied using displacement control of 3 mm per load stage at a loading speed of 1 mm/min, until failure. Displacements were measured at the positions of load application by linear variable displacement transducers (LVDTs). Strain gauges were mounted on tensile steel bars of each specimen in order to monitor the strain during loading.

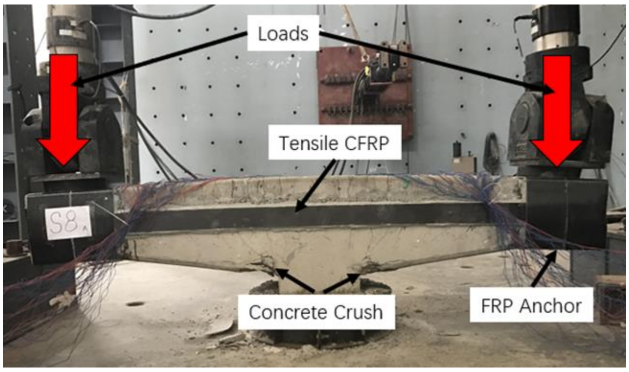

Fig. 3 Experimental test

Table 3 Experimental results

Beams	Steel yielding (kN)	Concrete crushing (kN)	Ultimate capacity (kN)	Ultimate failure mode
BREF	229.3	256.7	256.7	CC*
B1LI	329.6	350.5	376.6	AS*
B1L2	381.4	440.3	449.0	AS
B2L1	308.4	322.3	338.6	AS
B2L2	336.2	368.5	391.7	AS

*CC: Concrete crush; AS: Slipping between CFRP plate and anchor system

2.3 Test results

The reference beam BREF failed by concrete crushing in compression zone prior to steel yielding. The CFRP plate strengthened beams developed the flexural capacity by concrete crushing and ultimately failed by slipping of CFRP plates from the CFRP sheet anchors.

Table 3 summarizes the experimental results of all the test specimens. It presents the load points at the following stages: tensile steel yielding, concrete crushing, and ultimate failure. For the reference beam, a clear cracking point could be captured on the load-displacement diagram, however, for CFRP strengthened beams, no clear cracking point could be observed. Load-displacement diagrams of tested specimens are shown in Figs. 9-13.

3. Finite element modelling

A 3D finite element model was developed using a commercial FE package ABAQUS to simulate the structural behaviour of extended cap beams strengthened with CFRP composites. Following assumptions were made in the proposed finite element model: (a) steel reinforcement are fully bonded to concrete; (b) steel in extensions are appropriately connected to the original tensile steel; (c) Concrete crush occurs at a strain of 0.003; (d) Slipping of CFRP plates from CFRP sheet anchor occurs when the tensile force on CFRP exceed the maximum capacity of the anchor system. By taking advantage of symmetry, half of the beam was modelled, as shown in Fig. 4, for the purpose of reducing computational cost. Material properties used in the FE model were acquired from material tests in the experimental program. A rigid plate with a diameter of 300

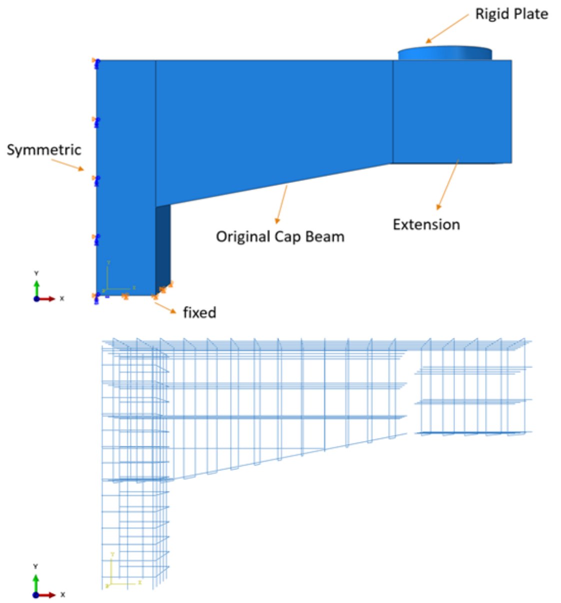

Fig. 4 Finite element modelling

mm, which was used in the experimental test as well, was placed on top surface for loading.

3.1 Modelling of concrete

The concrete damage plasticity (CDP) model was adapted for concrete modelling. The CDP model is a continuum model assuming the concrete has failure criteria: tensile cracking and compressive crushing. As shown in Fig. 5(a), for uniaxial tension, there is a linear relationship between stress and strain until reaching tensile strength of concrete, which represents the initiation of micro-cracking. Beyond the cracking point, the micro-cracking is simulated by a strain softening for the cracked concrete. For uniaxial compressed concrete, as shown in Fig. 5(b), the stress and strain maintain a linear relationship until reaching the initial yielding stress. Stress hardening and strain softening beyond the yielding can be defined by inputting compressive stress data as a tabular function of inelastic strain. Damage parameters (d_t and d_c) can be defined to represent reduction of elastic modulus, when the concrete is unloaded at any point on the strain softening branch, for both tension and compression.

In this study, a simplified compressive constitute model (Yang *et al*. 2014) was adapted to simulate compressive behaviour of concrete, as shown in Fig. 6. In this model, a key factor β_1 was implemented to represent the slopes of the ascending and descending branches. β_1 can be calculated from Eq. (1).

$$\beta_1 = 0.2\exp\left(0.73\xi\right) \quad for\ \varepsilon_c \le \varepsilon_0 \tag{1a}$$

$$\beta_1 = 0.41\exp\left(0.77\xi\right) \quad for\ \varepsilon_c > \varepsilon_0 \tag{1b}$$

Where ξ is equal to $(f_c'/f_0)^{0.67}(w_0/w_c)^{1.17}$, and the reference values of f_0 and w_0 are equal to 10 MPa and 2300 kg/m^3, respectively; ε_0 can be calculated using Eq. (2).

$$\varepsilon_0 = 0.0016\exp\left(240(f_c'/E_c)\right) \tag{2}$$

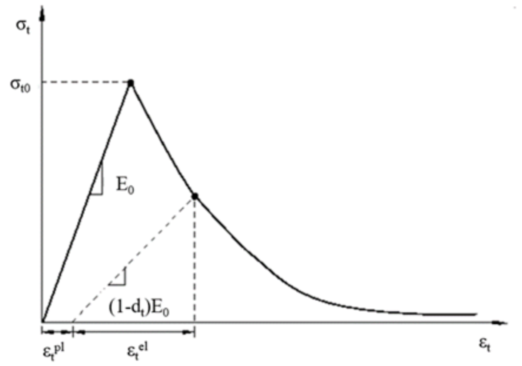

(a) Tension

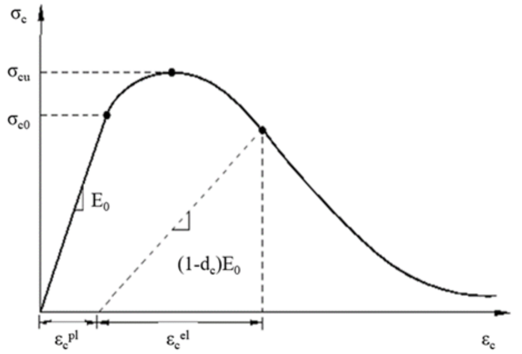

(b) Compression

Fig. 5 Uniaxial tensile and compressive stress-strain behavior of concrete (Dassault 2016)

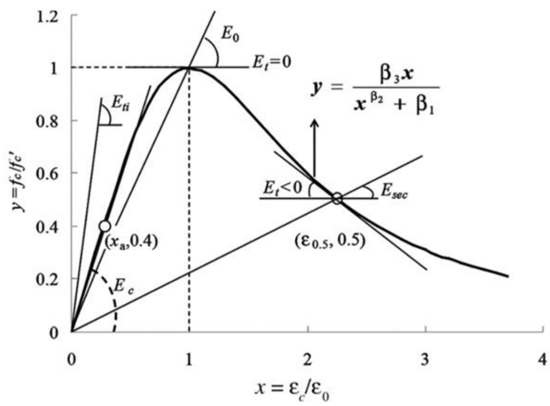

Fig. 6 Compressive behavior of concrete (Yang *et al*. 2014)

Where f_c' is compressive concrete strength; E_c is the compressive elastic modulus of concrete.

Stress strain relationship can be presented in Eq. (3).

$$f_c = \left[\frac{(\beta_1+1)\left(\frac{\varepsilon_c}{\varepsilon_0}\right)}{\left(\frac{\varepsilon_c}{\varepsilon_0}\right)^{\beta_1+1} + \beta_1}\right] f_c' \tag{3}$$

Where ε_c is the strain; f_c is the corresponding stress.

A bi-linear behaviour was assumed for concrete under uniaxial tension. Other factors required in CDP model were defined as following: dilation angle is 35°; a Poisson's ratio is 0.2; yielding parameter K_c is 0.667 and eccentricity is 0.01. Concrete was modelled with C3D8R element, a 3-D stress solid element with 8 nodes.

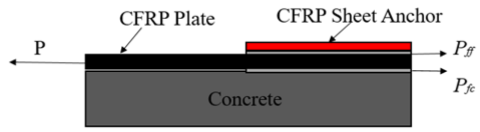

Fig. 7 Bonding mechanism of the anchored zone

3.2 Modelling of steel reinforcement

Steel reinforcement were assumed to have an elastic-perfectly plastic stress-strain relationship. Based on the assumption that steel reinforcement were fully bonded to concrete, the steel were embedded to the concrete without any slipping. T3D2, A 3-D truss element with 2 nodes was used to model steel reinforcement.

3.3 Modelling of CFRP composites

CFRP plates were modelled using a 4 nodes shell element, S4R, with the same properties shown in Table 2. For the region without CFRP sheet anchor, a layer of cohesive element was placed between the CFRP plates and concrete surface. Traction-separation damage was employed and the damage evolution was defined by fracture energy. It was later found having insignificant effect on ultimate capacity as the anchor strength dominated the ultimate failure.

For the anchored zones, CFRP plates were tied to the concrete and tensile force on CFRP plates were monitored during analysis. The analysis was terminated once the tensile force on CFRP plates exceeded the capacity of anchor system, which is predicted with an analytical approach (Singh *et al*. 2019). This represents slipping of the CFRP plates from the anchor.

An upper bound and a lower bound value were defined as the capacity of the CFRP sheet anchor system, as shown in Eq. (4). According to Fig. 7, tensile force carried by CFRP plates is equal to the sum of bonding force at concrete-FRP and FRP-FRP interface. The upper bound anchor capacity equals to the sum of maximum force the two interfaces could carry, which assuming both interfaces develop the capacity. The lower bound anchor capacity equals to two time the minimum of bond strength of the two interfaces, which assuming slippage occurs as one of the two interfaces develops its capacity

$$P_{upper} = P_{cf} + P_{ff} \tag{4a}$$

$$P_{lower} = 2 * min(P_{cf}, P_{ff}) \tag{4b}$$

Where P_{upper} is the upper bound value of anchor capacity; P_{lower} is the lower bound value of anchor capacity; P_{cf} is the bond strength of concrete-FRP interface; P_{ff} is the bond of FRP-FRP interface. P_{cf} and P_{ff} can be determined using Eq. (5) and Eq. (8) (Singh *et al*. 2019), respectively.

$$P_{fc} = \frac{b_f}{\gamma_{fd}}\sqrt{2\Gamma E_f t_f}\,\frac{L}{L_{cr}}\left(2 - \frac{L}{L_{cr}}\right) \quad L < L_{cr} \tag{5a}$$

$$P_{fc} = \frac{b_f}{\gamma_{fd}}\sqrt{2\Gamma E_f t_f} \quad L \geq L_{cr} \tag{5b}$$

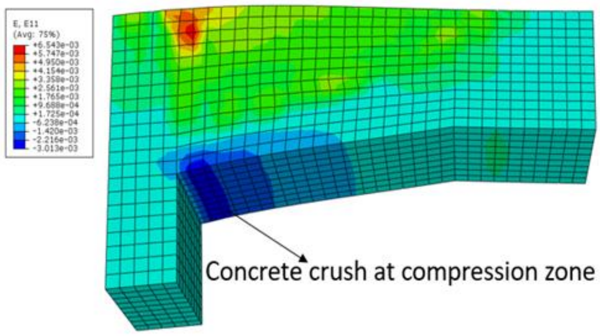

Fig. 8 Beam REF concrete crushing

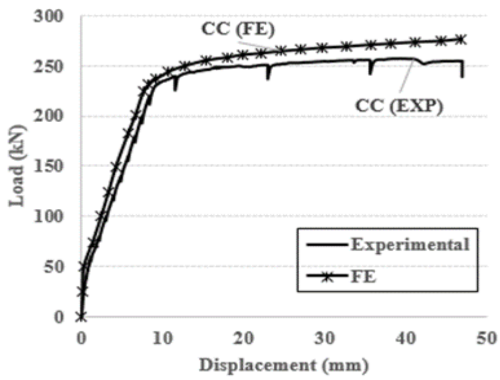

Fig. 9 Beam REF: FE vs experimental

Where b_f is width of CFRP plate; γ_{fd} is flexural strength reduction factor with a value of 1.0; Γ is concrete fracture energy; E_f is elastic modulus of CFRP plate; t_f is thickness of CFRP plate; L is bond length of CFRP plate, and L_{cr} is critical bond length of CFRP-concrete interface, which can be determined using Eq. (6).

$$L_{cr} = \frac{1}{\gamma_{Rd} f_{bd}}\sqrt{\frac{\pi^2 \Gamma E_f t_f}{2}} \tag{6}$$

Where γ_{Rd} is corrective factor equal to 1.25; f_{bd} is design FRP bond strength from Eq. (7).

$$f_{bd} = \frac{2\Gamma}{S_u} \tag{7}$$

Where S_u is fiber deformability matrix component which is equal to 0.25 mm.

$$P_{fc} = \frac{b_f}{\gamma_{fd}}\sqrt{2\Gamma E_f t_f}\,\frac{L}{L_{cr}}\left(2 - \frac{L}{L_{cr}}\right) \quad L < L_{cr} \tag{8a}$$

$$P_{fc} = \frac{b_f}{\gamma_{fd}}\sqrt{2\Gamma E_f t_f} \quad L \geq L_{cr} \tag{8b}$$

Where σ_r is adhesive tensile strength; σ_f is CFRP plate tensile strength and L_{crf} is critical length of FRP-FRP interface, which could be calculated using Eq. (9).

$$L_{crf} = \frac{3\sigma_f t_f}{2\sigma_r} \tag{9}$$

3.4 Finite element results

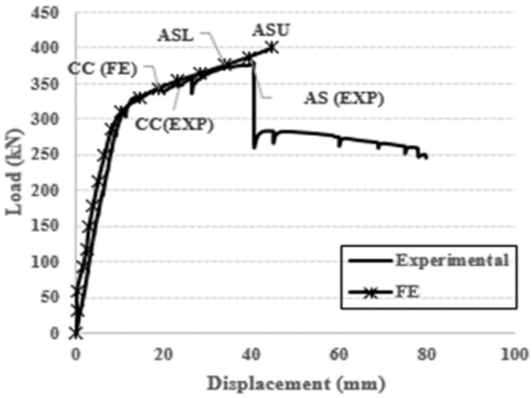

Fig. 10 Beam B1L1: FE vs experimental

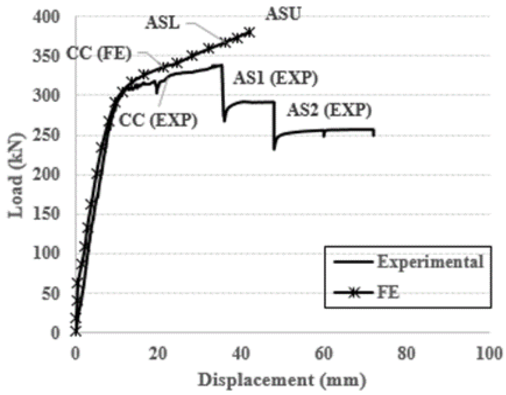

Fig. 12 Beam B1L2: FE vs experimental

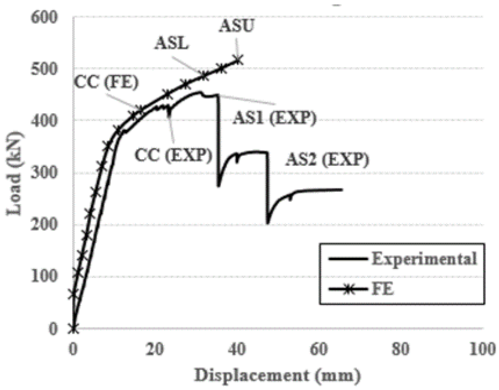

Fig. 11 Beam B2L1: FE vs experimental

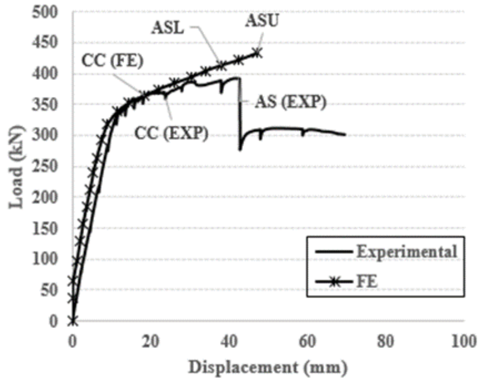

Fig. 13 Beam B2L2: FE vs experimental

3.4.1 Reference specimen BREF

The reference specimen BREF failed by concrete crushing in compression zone. The proposed finite element model was able to predict concrete crushing by assuming concrete crush at a strain of 0.003 as shown in Fig. 8. The concrete crushing load is indicated in Fig. 9, which shows the load-displacement response comparison between finite element results and experimental results.

The FE results showed slightly higher stiffness and slightly higher ultimate capacity than the experimental results, which attributes to the assumption that steel reinforcement were fully bonded to concrete.

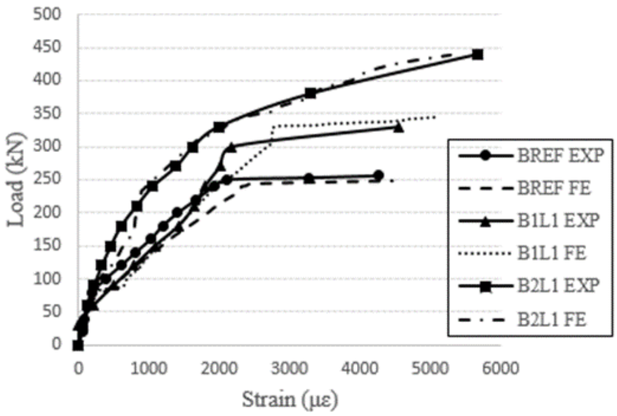

Fig. 14 Steel strain comparison (L1)

3.4.2 Beams strengthened with CFRP composites

Beams strengthened with one/two layers of CFRP plate at various locations developed the flexural capacity by concrete crushing prior to steel yielding. However, the ultimate failure of the strengthened beams failed by CFRP plate pulling out from the CFRP sheet anchor, which referred as anchor slippage. This failure mode was successfully captured using the proposed FE model by monitoring the tensile force on CFRP plates. Figs. 10-13 shows load-displacement response predicted using the proposed FE model for CFRP plate strengthened beams, alone with experimental results. ASU and ASL represents the upper and lower bound value of anchor slippage, respectively. In addition, concrete crushing is indicated for both FE and experimental results.

The same as the reference beam, the proposed FE model slightly overestimate the stiffness and ultimate capacity of the CFRP strengthened beam. For all the strengthened beams except B1L2, the experimental slippage occurred at a displacement between the lower and upper bound prediction using the anchor capacity dominated approach. For safety concern, the lower bound value is recommended to be adapted in analysis and design.

3.4.3 Strain analysis

The proposed FE model was verified using the strain data collected from the experimental test. Figs. 14-15 shows comparison between FE and experimental results in terms of strain on tensile steel, for CFRP location 1 and 2 respectively. Good agreements were achieved for all the tested specimens.

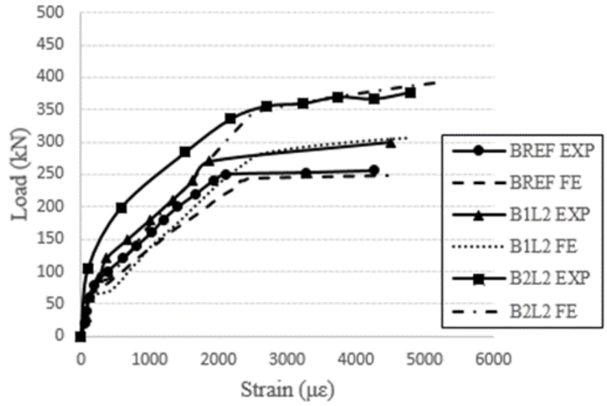

Fig. 15 Steel strain comparison (L2)

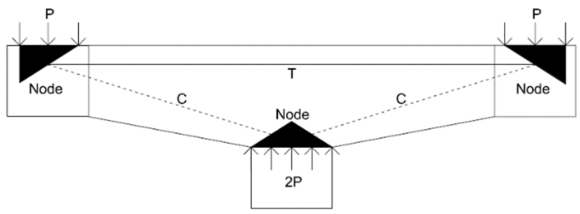

Fig. 16 Idealized geometry of proposed strut-and-tie model

4. Strut-and-tie based analytical approach

Change in geometry of a structural member causes a non-linear distribution of strains within the cross-section, which means the plan sections assumption cannot be applied. Strut-and-tie model, which consists of struts and ties connected at nodes, is widely used for strength prediction of such concrete members, as it allows for easy visualization of the force flows. In this section, a strut-and-tie based analytical model is developed and verified against the experimental results. It was found that the proposed analytical model is capable of predicting the failure mode and ultimate strength of proposed widening system.

The proposed analytical model was developed based on following assumptions: (a) Plain section assumption is not applicable due to change of cross-section along the beam; (b) Idealized hypothetical pin-jointed truss structure can be used to model the geometrical discontinued member; (c) Tensile steel reinforcement yield at ultimate state; (d) Horizontal stress on bottom node is at its maximum permitted value of 0.85 f'_c; (e) The limiting compressive stress in a strut crossed by a tie can be determined using Eqs. (14)-(15) (ASSHITO 2012); (f) Slipping of CFRP plates from CFRP sheet anchor occurs when the force on CFRP exceeds the anchor capacity.

4.1 Analysis procedure

After preliminary estimation of the truss model, as shown in Fig. 16, an iterative analysis is performed to predict the failure mode and calculate ultimate strength. A flow chart of proposed analysis procedure is shown in Fig. 17. For a given load P, force/stress/strain in each element is compared to the limited value, any of these values exceed the limit indicates failure of the beam. If the given load P

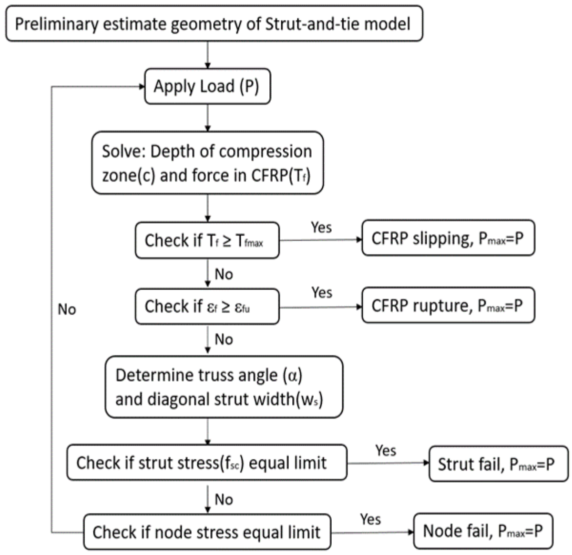

Fig. 17 Flow chart of proposed analytical model

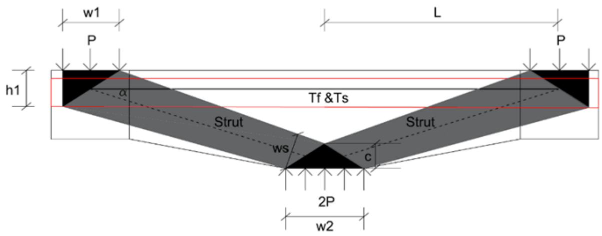

Fig. 18 Dimension of struts and nodes

doesn't cause any force/stress/strain beyond the limits, P should be increased. Limit checks are recommended to be performed but not limited in following order: (a). maximum capacity of the anchor system; (b) ultimate strain/stress on CFRP composites; (c) allowable stress in struts; (d) allowable stress in nodes.

The first step of strut-and-tie modelling is to select a suitable truss model. In this study, a simple truss model with direct diagonal struts from the loading points to the support is selected, and main tensile steel and CFRP composites served as ties. Geometry of the proposed strut-and-tie model is shown in Fig. 16. By establishing the basic truss geometry, location of the ties (tensile steel and CFRP composites) can be determined according to reinforcement detailing. Node dimensions w_1, h_1 and w_2, as shown in Fig. 18 can be determined by size of the support and loading pad.

By assuming horizontal stress on bottom node is at its maximum permitted value of $0.85f'_c$, tensile force on CFRP composites and depth of the bottom node "c" can be solved using following equilibrium equations.

$$A_s f_y + T_f = 0.85 f_c' bc \tag{10}$$

$$PL = A_s f_y \left(d_s - \frac{c}{2}\right) + T_f \left(d_f - \frac{c}{2}\right) \tag{11}$$

Where A_s is cross-section of tensile steel; f_y is yield strength of steel; T_f is tensile force in CFRP composites; $f'c$ is concrete compressive strength; b is width of the beam; c is depth of the bottom node; P is the applied load; L is the

Table 5 Summary of numerical predictions

Specimen	Experimental		Finite Element		Analytical		ACI
	P_{cc} (kN)	P_u (kN)	P_{cc} (kN)	P_u (kN)	P_{cc} (kN)	P_u (kN)	P_{cc}=P_u (kN)
BREF	256.7	256.7 (CC*)	263.5	263.5 (CC)	249.5	249.5 (CC)	229.5
B1L1	350.5	376.6 (AS)	339.3	376.0 (AS)	342.8	388.0 (AS)	335.4
B2L1	440.3	449.0 (AS)	409.4	487.8 (AS)	429.6	447.4 (AS)	386.6
B1L2	322.3	338.6 (AS)	409.4	487.8 (AS)	300.2	352.1 (AS)	306.1
B2L2	368.5	391.7 (AS)	370.5	419.1 (AS)	355.4	387.9 (AS)	342.5

*CC: Concrete crush; AS: Slipping between CFRP and anchor system

distance from the loading point to center of the beam; d_s is distance from centroid of tensile steel to bottom of the beam; d_f is distance from center of CFRP composites to bottom of the beam.

For CFRP plate strengthened beams, T_f is compared to the capacity of the CFRP sheet anchor system, which can be determined from Eq. (4b), to evaluate slipping failure of the anchor system. If adequate anchor capacity is provided, strain of CFRP composites shall be calculated according to Eq. (12) and compared to ultimate strain.

$$\varepsilon_f = \frac{T_f}{A_f E_f} \tag{12}$$

Where ε_f is strain of CFRP composites; A_f is area of CFRP composites; E_f is elastic modulus of CFRP composites.

As the depth of the bottom node "c" is known, angle between the diagonal strut and horizontal tie "α", width of strut "w_s" can be calculated from geometrical relationship. Compressive force on diagonal strut can be calculated using equilibrium of the top node. By dividing the compressive force by cross-section of the strut, stress in the strut can be calculated.

$$f_{sc} = \frac{C_{sc}}{w_s b} \tag{13}$$

Where f_{sc} is the stress in diagonal strut; C_{sc} is the compressive force in strut.

Strut stress is compared to the limit stress calculated from Eqs. (14)-(15) (ASSHITO 2012).

$$f_c = \frac{f_c'}{0.8 + 170\varepsilon_1} \leq 0.85 f_c' \tag{14}$$

$$\varepsilon_1 = \varepsilon_f + (\varepsilon_f + 0.002)cot^2(\propto) \tag{15}$$

Where f_c is the limit compressive stress in a strut crossed by a tie; ε_1 is the transverse tensile strain.

If the stress in the strut exceeds limit stress, it indicates failure of the strut. Node stress is calculated and compared to limit stress as typical strut-and-tie analysis. Nominal compressive strength of a nodal zone shall be calculated using Eq. (16) (AASHTO 2012).

$$f_{cn} = \phi \beta_n f_c' \tag{16}$$

Where ϕ is resistance for bearing on concrete; β_n is 0.85 for nodal zone bounded by struts; 0.75 for nodal zone anchoring one tie; 0.65 for nodal zone anchoring two or more ties.

Table 4 Analytical predictions

Beams	Experimental		Analytical	
	Concrete crush (kN)	Ultimate capacity (kN)	Strut failure (kN)	Ultimate capacity (kN)
BREF	256.7	256.7 (CC*)	249.5	249.5 (S)
B1LI	350.5	357.6 (AS)	342.8	388.0 (AS)
B1L2	440.3	449.0 (AS)	429.6	447.4 (AS)
B2L1	322.3	338.6 (AS)	300.2	352.1 (AS)
B2L2	368.5	391.7 (AS)	355.4	387.9 (AS)

*CC: Concrete crush; S: Strut failure; AS: Slipping between CFRP plate and anchor system

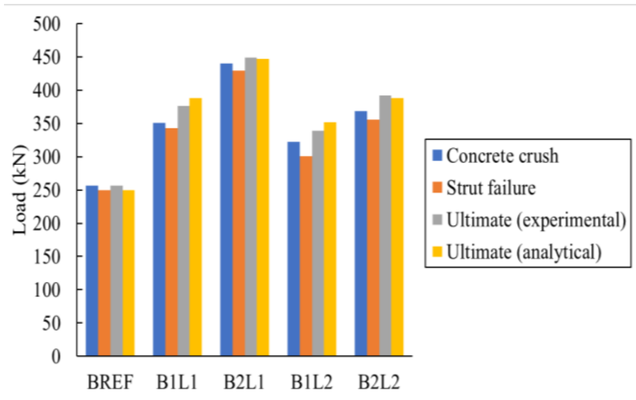

Fig. 19 Analytical results

4.2 Analytical results

Specimens with various strengthening systems from experimental study are analyzed with proposed analytical model. Failure modes and ultimate strength are summarized in Table 4 and plotted in Fig. 19.

Experimental results show that specimens strengthened by CFRP plates with CFRP sheet anchors failed by concrete crush followed by CFRP slippage. The smallest strut width in the proposed analytical model is at the location of the compression zone, where concrete crush occurred. Therefore, the analytical strut failure load is compared with concrete crushing load in experimental tests.

Reference specimen BREF, without any strengthening system, was analyzed using conventional strut-and-tie model. Analytical result shows good agreement with experimental results. Analytical prediction of ultimate load of BREF is slightly lower than the experimental results.

CFRP strengthened beams B1L1, B2L, B1L21and B2L2 failed by concrete crush followed by CFRP plate slippage in experimental test. Failure mode of these beams were

Table 6 Ratio between numerical predictions and experimental results

Specimen	P_{cc}			P_u	
	FE*/EXP	AM/EXP	ACI/EXP	FE/EXP	AM/EXP
BREF	1.03	0.97	0.89	1.03	0.97
B1L1	0.97	0.98	0.96	0.99	1.03
B2L1	0.93	0.98	0.88	0.99	1.00
B1L2	1.04	0.93	0.95	1.08	1.04
B2L2	1.01	0.96	0.93	1.07	0.99

*FE: Finite element; EXP: Experimental; AM: Analytical model

successfully predicted with proposed analytical model.

Analytical predictions of both concrete failure and CFRP slipping load show good agreement with experimental results.

5. Comparison and discussion

5.1 Sectional approach in current design guideline

A sectional approach is provided by American Concrete Institute (ACI 440 2017) to predict ultimate capacity of CFRP flexural strengthened RC beams. Following assumptions are made by the design guideline: Design calculations are based on the dimensions, internal reinforcing steel arrangement, and material properties of the existing member being strengthened; the strengthened beam has adequate shear strength; a plane section before loading remains plane after loading. Therefore, the strains in the steel reinforcement and concrete are directly proportional to their distance from the neutral axis; FRP composites are perfectly bonded to concrete; the shear deformation within the adhesive layer is neglected because the adhesive layer is very thin with only slight variations in its thickness; maximum allowable compressive strain in concrete is 0.003; tensile strength of concrete is neglected; FRP composites are perfect linear elastic until failure.

With above assumptions, flexural capacity of a section strengthened with CFRP composites can be determined by Eq. (17).

$$M_n = A_s f_s \left(d - \frac{\beta_1 c}{2}\right) + \Psi_f A_f f_{fe}(d_f - \frac{\beta_1 c}{2}) \qquad (17)$$

Where A_s and A_f are cross-section area of steel and CFRP reinforcement, respectively; f_s and f_{fe} are stress level from sectional analysis which could be determined using sectional stress and strain distribution diagram; d and d_f represents location of steel and CFRP reinforcement; Ψ_f is FRP strength reduction factor, which is 0.85 for flexure; β_1 is ratio of depth of equivalent rectangular stress block to depth of the neutral axis; c is depth of compression zone.

5.2 Comparison of numerical results

Ultimate strength predicted using finite element modeling, proposed analytical model and ACI sectional approach is summarized in Table 5 and plotted in Fig. 20.

Ratio between analytical predictions and experimental

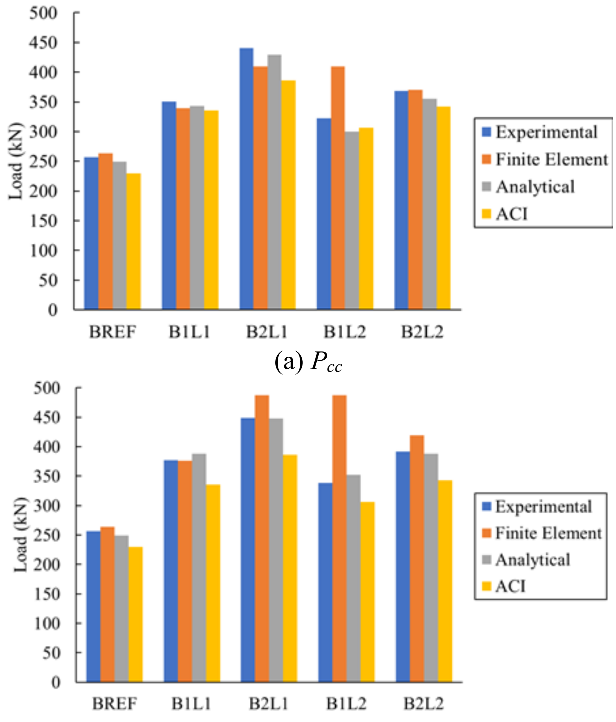

(a) P_{cc}

(b) P_u

Fig. 20 Comparison between different approaches

results are presented in Table 6. Regarding to concrete failure load, which is commonly used in engineering analysis and design, both finite element approach and proposed analytical model provide accurate predictions. Finite element and proposed analytical model give slight conservative ultimate capacity compared to experimental results for all tested strengthening systems. However, ACI sectional approach underestimates capacity of CFRP plate strengthened beam. Among the three approaches, the proposed analytical model gives the most accurate prediction of concrete failure load.

ACI sectional approach cannot predict the post-failure (CFRP rupture/slipping) load of the strengthened cap beams, since concrete crush is considered as ultimate failure of the beam. Both finite element and the proposed analytical approach can predict the CFRP slipping failure mode. Finite element model slightly overestimates post-failure load, as perfect bond of steel stiffens the beam. The proposed strut-and-tie model provides prediction of CFRP plate slipping load with an error less than 4%.

6. Conclusions

This paper presents a numerical study of hammer headed cap beams extended on verges and strengthened using CFRP plates along with CFRP sheet anchors. A 3-D FE model and a simple iterative based strut-and-tie analytical model were developed to predict failure mode and ultimate capacity of the extended beams.

The proposed finite element model is capable of predicting the structural behavior of extended beams strengthened with various strengthening systems in terms of failure mode, stiffness, yielding point and ultimate capacity, with good accuracy. Compared to experimental results, the proposed finite element model provides slightly higher stiffness and ultimate capacity. Stiffer behavior and higher ultimate capacity are attributed to the assumption of fully bond of steel reinforcement.

The proposed analytical model is capable of predicting the ultimate capacity (concrete compressive failure) of extended beams strengthened with various strengthening systems. Among finite element approach, proposed analytical model and ACI sectional approach, the proposed strut-and-tie based analytical provides the most accurate prediction of the concrete compressive failure load. For beams strengthened with flexural CFRP plates and CFRP sheet anchor system, the proposed analytical model can predict the CFRP slipping load with an error less than 4%.

Acknowledgments

The authors gratefully acknowledge the financial support of Shandong Luqiao Group. The authors would also like to acknowledge the work of the technicians at Shandong Jiaotong University and the CFRP technical advice by Horse construction Co. Ltd.

References

AASHTO (2012), AASHTO LRFD Bridge Design Specifications, American Association of State Highway and Transportation Officials, Washington, DC, USA.

ACI 440 (2017), ACI 440.2R-17, Guide for the Design and Construction of Externally Bonded FRP Systems for Strengthening Concrete Structures, American Concrete Institute, Farmington Hills, MI, USA.

ACI 447 (2018), ACI 447.1R-18, Report on the Modeling Techniques Used in Finite Element Simulations of Concrete Structures Strengthened Using Fiber-Reinforced Polymer (FRP) Materials, American Concrete Institute, Farmington Hills, MI, USA.

Andermatt, M.F. and Lubell, A. (2013), "Strength modelling of concrete deep beams reinforced with internal fiber-reinforced polymer", *ACI Struct. J.*, **110**(4), 595-605. https://doi.org/10.14359/51685745.

Biolzi, L., Ghittoni, C., Fedele, R. and Rosati, G. (2013), "Experimental and theoretical issues in FRP-concrete bonding", *Constr. Build. Mater.*, **41**, 182-190. https://doi.org/10.1016/j.conbuildmat.2012.11.082.

Dassault Systèmes (2016), ABAQUS 2016 Documentation. Providence, RI., USA.

Eamon, C.D., Jensen, E.A., Grace, N.F. and Shi, X. (2012), "Life-cycle cost analysis of alternative reinforcement materials for bridge superstructures considering cost and maintenance uncertainties", *J. Mater. Civil Eng.*, **24**(4), 373-380. https://doi.org/10.1061/(ASCE)MT.1943-5533.0000398.

Hag-Elsafi, O., Lund, R. and Alampalli, S. (2002), "Strengthening of a bridge pier cap beam using bonded FRP composite plates", *Compos. Struct.*, **57**(1-4), 393-403. https://doi.org/10.1016/S0263-8223(02)00107-1.

Jawdhari, A. and Harik, I. (2018), "Finite element analysis of RC beams strengthened in flexure with CFRP rod panels", *Constr. Build. Mater.*, **163**, 751-766. https://doi.org/10.1016/j.conbuildmat.2017.12.139.

KwaZulu-Natal Department of Transport (2017), Tongati River Bridge Widening on Main Road P714-SAICE 2017 Awards Category: Technical Excellence, Civil Engineering, Siviele Ingenieurs Wise, 18-18.

Lu, W., Hwang, S. and Lin, I. (2010), "Deflection prediction for reinforced concrete deep beams", *Comput. Concrete*, **7**(1), 1-16. https://doi.org/10.12989/cac.2010.7.1.001.

Luo, Y., Li, A. and Kang Z. (2012), "Parametric study of bonded steel–concrete composite beams by using finite element analysis", *Eng. Struct.*, **34**, 40-51. https://doi.org/10.1016/j.engstruct.2011.08.036.

Mihaylov, B., Bentz, E. and Collins, M. (2013), "Behavior of deep beams with large headed bars", *ACI Struct. J.*, **110**(6), 1013-1021. https://doi.org/10.14359/51686156.

Mostafa, A.A. and Razaqpur, A.G. (2017), "Finite element model for predicting post delamination behavior in FRP-retrofitted beams in flexure", *Constr. Build. Mater.*, **131**, 195-204. https://doi.org/10.1016/j.conbuildmat.2016.11.066.

Panjehpour, M., Ali, A., Voo, Y. and Aznieta, F. (2014), "Modification of strut effectiveness factor for reinforced concrete deep beams strengthened with CFRP laminates", *Materials de Construction*, **64**(314), 1-8. https://doi.org/10.3989/mc.2014.02913.

Park, S. and Aboutaha, R. (2009), "Strut-and-tie method for CFRP strengthened deep RC members", *J. Struct. Eng.*, **135**(6), 632-643. https://doi.org/10.1061/(ASCE)0733-9445(2009)135:6(632).

Rafeeqi, S. and Ayub, T. (2012), "Behavior of reinforced concrete beams detailed for shear in compliance with compressive force path method", NED University Journal of Research, **X**(1), 13-30.

Rowan, A. and Thomson, L. (2018), "Olifants River Bridge widening", *MATEC Web of Conferences*, **199**, 10007. https://doi.org/10.1051/matecconf/201819910007.

Singh, A., Castillo, E. and Ingham, J. (2019), "FRP-FRP bond characterization and force-based bond length model", *Compos. Struct.*, **210**, 724-734. https://doi.org/10.1016/j.compstruct.2018.12.005.

Thomas, J. and Ramadass, S. (2019), "Prediction of the load and deflection response of concrete deep beams reinforced with FRP bars", *Mech. Adv. Mater. Struct.*, 1-24. https://doi.org/10.1080/15376494.2018.1549292.

Wu, Y.F., Wang, Z., Liu, K. and He, W. (2009), "Numerical analyses of hybrid-bonded FRP strengthened concrete beams", *Comput.-Aid. Civil Infrastr. Eng.*, **24**(5), 371-384. https://doi.org/10.1111/j.1467-8667.2009.00596.x.

Yang, K.H., Mun, J.H., Cho, M.S. and Kang, T.K. (2014), "Stress-strain model for various unconfined concretes in compression", *ACI Struct. J.*, **11**(4), 819-826. https://doi.org/10.14359/51686631.

Zhang, S. and Teng, J. (2016), "End cover separation in RC beams strengthened in flexure with bonded FRP reinforcement: simplified finite element approach", *Mater. Struct.*, **49**, 2223-2236. https://doi.org/10.1617/s11527-015-0645-z.

CC